Fusicoccane Diterpenes from *Hypoestes forsskaolii* as Heat Shock Protein 90 (Hsp90) Modulators

Massimiliano D'Ambola,[†,#] Lorenzo Fiengo,[†,#] Maria Giovanna Chini,[†] Roberta Cotugno,[†] Ammar Bader,[§] Giuseppe Bifulco,[†] Alessandra Braca,[⊥,‖] Nunziatina De Tommasi,[*,†] and Fabrizio Dal Piaz[†,‡]

[†]Dipartimento di Farmacia, Università degli Studi di Salerno, via Giovanni Paolo II 132, 84084 Fisciano (SA), Italy

[‡]Dipartimento di Medicina, Chirurgia e Odontoiatria "Scuola Medica Salernitana", Università degli Studi di Salerno, via Giovanni Paolo II 132, 84084 Fisciano (SA), Italy

[§]Department of Pharmacognosy, Faculty of Pharmacy, Umm Al-Qura University, 21955 Makkah, Saudi Arabia

[⊥]Dipartimento di Farmacia, Università di Pisa, via Bonanno 33, 56126 Pisa, Italy

[‖]Centro Interdipartimentale di Ricerca "Nutraceutica e Alimentazione per la Salute", Università di Pisa, via del Borghetto 80, 56124 Pisa, Italy

Dedicated to Dr. Rachel Mata, National Autonomous University of Mexico, Mexico City, Mexico, and Dr. Barbara N. Timmerman, University of Kansas, for their pioneering work on bioactive natural products

ABSTRACT: Ten new (**1-10**) and six known (**11-16**) fusicoccane diterpenes were isolated from the roots of *Hypoestes forsskaolii*. The structural characterization of **1-10** was performed by spectroscopic analysis, including 1D- and 2D-NMR, ECD, and HRESIMS experiments. From a perspective of obtaining potential Hsp90α inhibitors, the isolates were screened by Surface Plasmon Resonance (SPR) measurements and their cytotoxic activity was assayed using Jurkat and HeLa cancer cells. Compound **6**, 18-hydroxyhypoestenone, was shown to be the most active compound against Hsp90, and its interactions were studied also by biochemical and cellular assays, and by molecular docking.

Hypoestes forsskaolii (Vahl) R. Br. (Acanthaceae) is a perennial bushy and leafy herb widely distributed in several African countries as well as in high mountains of the Arabian Peninsula.[1] This species was named by the Danish-Norwegian botanist Martin Vahl (1749-1804) in honor of the Swedish naturalist Peter Forsskål (1732-1763), who was an associate of Carl Linnaeus. In an elegant taxonomic study of the genus *Hypoestes* in South Africa, the authors highlighted the variability of species epithet as derived from the name Forsskål, which is spelt in many different ways including Forsskål, Forskål, and Forsskåhl. Latinization of this name has also contributed several orthographic variants, so the epithet includes *forskaolii*, *forskalei*, *forskolii*, *forskohlii*, and *forskaolea*.[2] In Saudi Arabia the plant has several popular names, including "Nadgha", "Majra", "Qumaylah",[3] and is used popularly as a natural insecticide; in particular, a decoction of this plant is used to wash goats infested by fleas, while the fresh leaves are added to milk to attract and to kill flies. The fresh leaves are also applied to wounds to accelerate healing and the fresh stems are used to massage the scalp to kill head lice and to destroy their eggs.[3] Plants belonging to *Hypoestes* genus, including *H. forsskaolii*, are the main source of fusicoccane diterpenes,[4-6] characterized by a complex 5-8-5-diciclopentacyclooctane nucleus, so far identified in bacteria, algae, fungi, higher plants, and insects,[7,8] but also isopimarane,[9] and labdane[10] diterpenes have been reported. The main biological activities reported for the fusicoccanes are antimicrobial[11] and cytotoxic effects.[12]

Herein are reported the isolation and structural characterization, obtained by 1D- and 2D-NMR spectroscopy and mass spectrometry data, of ten new (**1-10**) and six known (**11-16**) fusicoccane diterpenes from the roots of *H. forsskaolii* (Chart 1). In order to obtain potential Hsp90 inhibitors, the isolates were screened by Surface Plasmon Resonance (SPR) measurements; biochemical and cellular assays, as well as molecular docking were used to assess their activity.

The multiple functions played by the molecular chaperone Hsp90, particularly in response to different stresses, make this protein a promising target for several therapeutic approaches.[13] The modulation of Hsp90 thus has been proposed as an efficient strategy to combat pathologies such as multiple cancer types,[14,15] neurodegenerative disorders,[16] and viral infections.[17] Many plant

secondarymetabolites, belonging to different classes, have been shown to interact efficiently with Hsp90, inhibiting its activity in cancer cells and exerting significant antiproliferative and/or proapoptotic actions.[18-20]

RESULTS AND DISCUSSION

The roots of *H. forsskaolii* were extracted with solvents of increasing polarity. After separation of the $CHCl_3$ and $CHCl_3$-MeOH extracts by column chromatography over silica gel, Sephadex LH-20, and then RP-HPLC, ten new (**1-10**) and six known fusicoccane diterpenes (**11-16**) were purifed.

The HRESIMS of compound **1** gave a $[M + Na]^+$ peak at *m/z* 309.2191. The resulting molecular formula was determined to be $C_{20}H_{30}O$, showing six degrees of unsaturation. The ^1H NMR spectrum (Table 1) exhibited the presence of two methyl singlets (δ 1.05, 1.57), two methyl doublets (δ 0.95, 1.08), an exocyclic methylene (δ 4.71, 4.79), a sp^2 proton triplet (δ 5.51), five methylenes, and five methines. The ^{13}C NMR spectrum of **1** (Table 1) displayed 20 carbon signals that were assigned for four methyls (δ 16.0, 21.9, 23.7, 24.0), five methylenes (δ 26.0, 26.3, 31.9, 35.0, 43.0), five methines (δ 32.3, 42.9, 45.0, 47.7, 56.6), a sp^2 methylene (δ 103.1), a methine double bond (δ 127.9), a keto carbonyl group (δ 225.0), and three quaternary carbons (δ 51.4, 137.1, 148.0). The sequence H_2-2—H_2-5, H-5—H-7, H-9—H_2-13 was provided by 1D-TOCSY and COSY experiments, while all protons directly bonded to carbon atoms were assigned on the basis of HSQC spectroscopic cross peaks. The presence of an isopropyl moiety was revealed by the signals at δ 0.95 (3H, d, J = 6.5 Hz, Me-19)/23.7 (C-19), 1.08 (3H, d, J = 6.5 Hz, Me-20)/24.0 (C-20), and 1.86 (1H, m, H-18)/32.3 (C-18), and confirmed by 1D-TOCSY and COSY correlations. The HMBC cross peaks H_2-13—C-14, Me-15—C-14, H_2-10—C-8, Me-17—C-8, H_2-16—C-3, H_2-16—C-5, H_2-2—C-7, and H_2-2—C-11, suggested a keto carbonyl group location to be at C-14, a double bond at C-8/C-9, and an exocyclic double bond at C-4. These data were consistent with the occurrence of a

fusicoccane diterpene.[4] The relative configuration of **1** was assigned by 1D-ROESY correlations between δ 1.05 (Me-15) and 1.86 (H-18), 2.56 (H-3), and 3.31 (H-7), locating these protons on the same side of the molecule. Thus, the structure of **1** was elucidated as fusicocc-4,(16),8,(9)-dien-14-one.

The molecular formula of compound **2** ($C_{20}H_{30}O$) was determined from its HRESIMS ($[M + Na]^+$ ion at *m/z* 309.2178) and ^{13}C NMR data, showing it to be an isomer of **1**. Comparison of the NMR spectroscopic data of **2** with those of **1** (Table 1) indicated that these compounds differ only in one double bond position. In fact, the ^1H NMR spectrum of **2** showed the presence of a sp^2 methine singlet at δ 5.59 and a methyl doublet at δ 1.03 (J = 7.0 Hz) instead of an exocyclic methylene as in **1**. Moreover, three spin systems, H-7—Me-16, H-9—H-13, H-9—Me-20, were recognized from the 1D-TOCSY and COSY spectroscopic analysis. The position of the double bonds was ascertained by the HMBC correlations between H-2—Me-15, H-2—C-4, H-2—C-7, H-2—C-14, H-9—C-7, H-9—C-11, and H-9—Me-17. Consequently, **2** was characterized as fusicocc-2,(3),8,(9)-dien-14-one.

Compound **3** was assigned a molecular formula $C_{20}H_{32}O$ by its HRESIMS acquired in the positive-ion mode (*m/z* 289.2528). This information, along with ^{13}C NMR data (Table 1), was sorted into twenty carbons as four methyls, seven methylenes, of which one had a sp^2 carbon, five methines, a hydroxymethine, and three quaternary carbons, of which one was a sp^2 carbon, and led to the determination of five indices of hydrogen deficiency and a fusicoccane skeleton for **3**.[21] The NMR spectra of **3** showed the resonances for an epoxy ring (δ_H 2.88, δ_C 62.8 and 68.1) that was located at C-8/C-9, on the basis of cross peaks in the COSY and 1D-TOCSY spectra between H-9—H_2-10—H-11—H-12—H_2-13—H_2-14 and from thecorrelations observed in the HMBC spectrum between H-9 (δ_H 2.80) and C-10 (δ_C 26.0), C-17 (δ_C 20.0), and Me-17 (δ_H 1.09) and C-7 (δ_C 48.0), C-8 (δ_C 62.8), and C-9 (δ_C 68.1), H-11 (δ_H 1.77) and C-9 (δ_C 68.1). The signals observed in the NMR spectra at δ 4.77, 4.83 (H_2-16)/103.2 (C-16) and 157.0 (C-4) suggested the presence of an exocyclic methylene group, which was located at C-4 on the basis of the proton and carbon chemical shifts of ring A and key HMBC correlations between H-5—C-4 and H-6—C-4. The relative configuration of

compound **3** was obtained on the basis of 1D-ROESY data. The β-orientation of H-9, H-11, H-12, and Me-17 was indicated by ROE cross peaks among spatially related protons, particularly H-9 with H-11, and Me-17 and H-12 with H-9 and H-11. The α-orientation of H-3, H-7, and Me-15 was deduced by ROE correlations between δ 0.89 (Me-15) and δ 2.30 (H-7) and δ 2.56 (H-3). From these results, the structure of compound **3** was determined as 8(9)α-epoxy-fusicocc-4,16-ene.

The HRESIMS of compound **4** showed a protonated molecular ion peak at *m/z* 315.1959 $[M + H]^+$, consistent with a molecular formula of $C_{20}H_{26}O_3$, requiring eight degrees of unsaturation. The ^{13}C NMR spectrum (Table 1) displayed 20 signals that were sorted into five methyls, three methylenes, five methines, of which two were linked to sp^2 carbons, and seven quaternary carbons, including two keto carbonyl groups. The ^1H NMR (Table 1) showed the presence of two trisubstituted double bonds at δ 5.53 and 5.79, two methyl singlets at δ 1.28 and 1.85, a methyl doublet at δ 0.86 (J = 6.8 Hz), and signals of an isopropyl group at δ 1.15 (3H, d, J = 6.5 Hz, Me-20)/20.7 (C-20), 1.19 (3H, d, J = 6.5 Hz, Me-19)/22.0 (C-19), and 2.65 (1H, m, H-18)/28.5 (C-18). This inferred again the presence of a fusicoccane diterpene.[12] From the 1D-TOCSY, COSY, and HSQC spectroscopic data, the spin systems C-4—C-16, C-6—C-7, C-9—C-10, C-18—C-20 could be established. The elucidation of the whole skeleton in **4** was achieved on the basis of HSQC and HMBC correlations. HMBC correlations between Me-16—C-3, Me-16—C-5, H-6—C-3, H-10—C-11, H-13—C-11, Me-15—C-11 confirmed that C-3 and C-11 are oxygenated and the presence of a C-3/C-11 oxide bridge was thus established. The Me-16 relative configuration was determined by 1D-ROESY experiments that showed cross peaks between Me-16 and H-7 and Me-15 and Me-16. Thus, **4** was characterized as 3(11)-epoxy-fusicocc-8,(9),12,(13)-dien-5,14-dione.

Compound **5** was assigned the molecular formula, $C_{20}H_{30}O_3$, from the sodiated molecular ion peak at *m/z* 341.2192. Compared with **2**, three more oxygenated carbons were present, at δ 65.3 (C-8), 66.0 (C-9), and 80.0 (C-4), and a double bond was absent (Table 2). In the ^1H NMR spectrum of **5** (Table 2) a signal at δ 2.93 (1H, dd, J = 9.0, 6.0 Hz) allowed the presence of an epoxy ring to be established, while the methyl singlet at δ 1.10 replaced the methyl doublets at δ 1.03 in **2**. The

epoxy group was located at C-8/C-9 from the HMBC correlations between H-7—C-3, H-7—C-8, H-7—Me-17, H-9—C-10, H-11—C-9, Me-17—C-8, and Me-17—C-9, while the hydroxy group was positioned at C-4 from the HMBC cross peaks between H-2—C-4, H-7—C-4, and Me-16—C-4. The relative configuration of compound **5** was deduced by coupling constant data and the 1D-ROESY spectrum. Particularly, the position of the hydroxy group at C-4 was inferred from the ROE correlations between Me-16 and Me-17 and between Me-17 and H-11. Therefore, **5** was assigned as 8(9)α-epoxy-4α-hydroxy-fusicocc-2,3-en-14-one.

Compound **6** (molecular formula $C_{20}H_{28}O_3$) showed in the HRESIMS a sodiated ion peak at *m/z* 339.1931 and a protonated ion peak at *m/z* 317.2114, respectively. Comparison of its NMR data (Table 2) with those of hypoestenone[4] suggested **6** as being most likely the C-18 hydroxy derivative of hypoestenone, since the 2D NMR spectra, including COSY, HSQC, and HMBC experiments, showed the presence of two methyl singlets instead of two methyl doublets at C-18. The relative configuration of **6** was assigned by comparison of ^{1}H—^{1}H coupling constants and chemical shifts with those of hypoestenone.[4] Therefore, the structure of **6** was determined as 18-hydroxyhypoestenone. The absolute configuration of **6** was determined by the comparison between the experimental electronic circular dichroism (ECD) spectrum and the TDDFT-predicted curve calculated at the quantum mechanical (QM) level. As previously reported,[22,23] an extensive conformational search related to one of the possible enantiomers (**6a** and **6b**, Chart 2) was required for the subsequent phases of computation of the ECD spectra. First, the conformational search was performed at the empirical level (molecular mechanics, MM), combining Monte Carlo molecular mechanics (MCMM), low-mode conformational sampling (LMCS), and molecular dynamics (MD) simulations[24] (Experimental Section). The MM-sampled conformers of the one possible enantiomer (**6a**) were subjected to geometry and energy optimization steps at the MPW1PW91/6-31G(d) density functional level of theory (DFT) and then the TDDFT-predicted curve was calculated at the MPW1PW91/6-31G(d,p) functional/basis set in EtOH (IEFPCM), to reproduce the effect of the solvent.[25] Comparison of the experimental and calculated ECD curve of **6a** showed it to be similar

to the experimental ECD of **6** (Figure 1). Therefore, **6a** is proposed as the correct stereostructure for **6** and was assigned as shown in Chart 2.

From the NMR and MS data of compound **7** the molecular formula $C_{20}H_{28}O_3$ (HRESIMS at *m/z* 339.1911 $[M + Na]^+$) was determined, with **7** being an isomer of **6**. Analysis of the NMR data indicated that **7** differs from **6** by the different position of the hydroxy group. The ^1H and ^{13}C NMR spectra of **7** (Table 2) revealed the presence of a hydroxymethylene group (δ_H 3.38, dd, J = 11.0, 6.0 Hz, 3.56, dd, J = 11.0, 3.0 Hz, δ_C 67.7) at C-19 instead of a methyl group in **6**. Unfortunately, due to the limited amount isolated the relative configuration could not be defined. Thus, compound **7** was elucidated as 19-hydroxyhypoestenone.

Compound **8** ($C_{20}H_{26}O_3$) showed a $[M + H]^+$ at *m/z* 315.1960. Its ^1H NMR spectrum (Table 3) showed three methyl singlets at δ 1.18, 1.80, and 1.96, a hydroxymethine group at δ 4.81, a typical isopropyl group of a fusicoccane diterpenoid, and a trisubstituted double bond (δ 5.84 s). The ^1H NMR spectrum of **8** combined with the observation from the 1D-TOCSY and COSY experiments suggested the sequences H-9—H-11 and H-18—Me-20, while the signals of H-2 and H-6 were two doublets of doublets. HMBC correlations between H-2—C-5, H-6—C-8, H-11—C-3, H-11—C-13, Me-16—C-4, Me-16—C-5, Me-17—C-7, Me-17—C-9, and Me-18—C-12 permitted the sp^2 double bond to be located between C-12 and C-13, two tetrasubstituted double bonds between C-3 and C-4 and C-7 and C-8 and two keto carbonyl groups at C-5 and C-14. The relative configuration of H-9 was slightly ambiguous since no correlations were observed in the 1D-ROESY spectra, when irradiating Me-15 and H-11. The NMR spectra of **8** were also recorded in $CDCl_3$ (Table 3) to obtain different proton chemical shifts, but also in this case the H-9 irradiation failed. Thus, the structure of **8** was characterized as 9-hydroxy-fusicocc-3,(4),7,(8),12,(13)-trien-5,14-dione.

Compound **9** displayed a molecular formula $C_{20}H_{32}O$ from its HRESIMS (*m/z* 289.2528 $[M + H]^+$) and NMR data (Table 3). The carbon resonances at δ 124.4 and 131.0, which were assigned to an olefinic group based on COSY, HSQC, and HMBC data, and accounted for one degree of unsaturation, suggested the presence of four rings in the molecule of **9**. The results obtained from

1D-TOCSY and COSY experiments established the connectivity of protons H-5—H-7, H-9—H-14, and H-12—H-20. The elucidation of the whole skeleton from the above subunits was achieved using HSQC and HMBC correlations, which also allowed the assignment of all resonances in the ^{13}C NMR spectrum of the pertinent carbons. In the ^{13}C NMR spectrum, two signals at 63.4 and 69.0 ppm showed the presence of an epoxy ring, which was located at C-3/C-4 on the basis of a HMBC experiment. In the latter, key correlation peaks between H-2—C-3, H-7—C-3, H-7—C-4, H-11—C-1, H-11—C-8, H-11—C-9, H-14—C-1, H-14—C-12, Me-16—C-3, Me-16—C-4, Me-16—C-5 were observed. The relative configuration of the stereogenic centers of **9** was established by 1D-ROESY experiments. The Me-15 proton signal at δ 0.95 showed ROE correlations with the signals at δ 3.18 (H-7), while the Me-16 signal irradiation produced a weak correlation with H-11. Therefore, the structure of **9** was defined as 3(4)-epoxy-fusicocc-8,9-ene.

Compound **10** exhibited a molecular formula of $C_{20}H_{26}O_5$ as deduced from the HRESIMS (*m/z* 347.1855) and NMR data, accounting for eight degrees of unsaturation, of which four were attributable to an α,β-unsaturated carbonyl group and two keto carbonyl groups; thus, the structure of **10** was tetracyclic. The ^{13}C NMR data (Table 3) of **10** established the presence of an α,β-unsaturated carbonyl group, two keto carbonyl groups, three quaternary carbons bearing oxygen, a hydroxymethine, two methines, four methylenes, and five methyls. Analysis of the ^{1}H NMR spectrum (Table 3) showed an isopropyl group, three singlet methyl groups, with one linked to a double bond, four methylenes, a methine, and a hydroxymethine proton. The 1D-TOCSY and COSY experiments were used to establish the presence of the three spin systems H_2-6—H-7—H_2-2, H-9—H_2-10, and H-18—Me-20, demonstrating that **10** has the same ring A of hypoestenone,[4] while the other rings were points of difference. The HSQC spectrum supported these data, showing, in particular, a methine bearing a hydroxy group (δ_H 4.18, δ_C 79.7). The HMBC experiment displayed cross peaks between H_2-6—C-3, H_2-6—C-5, H_2-6—C-7, and H_2-6—C-8, while the Me-17 signal at δ 0.86 displayed correlations between δ 39.7 (C-7), 84.4 (C-8), and 79.7 (C-9), the Me-15 signal at δ 1.29 correlated with C-1 (81.0), C-2 (35.2), and C-14 (211.3), δ 2.73 (H-13b) and

2.54 (H-2b) correlated with 81.0 (C-1), so it was possible to hypothesize the presence of an ether linkage between C-1 and C-8. On the other hand, HMBC correlations were also observed between H-9 and C-10, C-11, and C-12, between H_2-13 and C-1, C-12, C-18, and two keto carbonyl groups located at C-11 and C-14, while H-18 showed correlations with C-13, Me-19, and Me-20, leading the proposal of an additional five-membered epoxy ring occurring at C-9 and C-12. The 1D-ROESY irradiation of Me-17 affected H-9 (and vice versa) and H-3, thus indicating that they are on the same side of the molecule. Thus, **10** was characterized as 1(11)-*seco*-1(8),9(12)-diepoxide-fusicocc-3,4-en-5,11,14-trione.

Deoxyhypoestenone (**11**),[5] hypoestenone (**12**),[4] dehydrohypoestenone (**13**),[5] 8(9)α-epoxyhypoestenone (**14**),[4] 8(9)α-epoxy-12(13)-anhydrohypoestenone (**15**),[21] and hypoestenonol B (**16**)[6] were also purified and identified by comparison of their spectroscopic data with those of the literature.

The affinity towards the molecular chaperone Hsp90α was assayed by SPR for the isolated compounds, except for **7**, as it was purified only in a limited amount; 17-AAG and radicicol were used as positive controls.[26] This SPR assay permitted the thermodynamic and kinetic parameters to be obtained of the fusicoccane/Hsp90α complex formations. Seven (**2**-**6** and **10**-**11**), out of the fifteen tested compounds, were observed to interact with the protein (Table 4): among them, compounds **2**, **6**, and **11** showed the greatest affinities towards the chaperone, as inferred by the measured K_D values falling in the 10-30 nM range. Due to the limited number of tested compounds and their structural features, a reliable structure-activity relationship study could not be established. The obtained data suggested that the interaction between the fusicoccane diterpenoid tested and Hsp90α could involve multiple sites in their structures.

On the basis of the ability of several of these compounds to bind Hsp90α, the potential antiproliferative activity of compounds **1**-**6** and **8**-**16** was evaluated using the human HeLa (cervical carcinoma) and Jurkat (human T-cell lymphoma) cell lines. The cells were incubated for 48 h with increasing concentrations of fusicoccanes (10-150 μM) and cell viability was determined by a MTT

proliferation assay.[27] While all compounds showed IC_{50} values of > 20 μM for both cancer cell lines, compound **6** demonstrated an IC_{50} value of 18 ± 1 μM in the HeLa cell line (Table S1, Supporting Information). Thus this compound was choosen for further biological studies. Notably, compound **6** did not show cytotoxic activity on non-tumor human peripheral blood mononuclear cell line (PBMC) up to 100 μM.

The mechanism of action of cancer cell viability inhibition exhibited by **6** was investigated by incubating HeLa cells for 48 h with concentrations close to the IC_{50} value of **6** (10 and 20 μM) and analyzed by flow cytometry. The treatment caused a G_2/M cell cycle arrest (Figure 2A). Hsp90α inhibition induced G_2/M arrest by affecting, directly or indirectly, the levels and the phosphorylation state of several cyclins and cyclin-dependent kinases (CDKs).[28,29] On this basis, the cell cycle arrest exerted by **6** was studied by evaluating the expression of these proteins. The results of Western blotting (Figure 2B) indicated that cell cycle arrest in G_2/M phase as observed for the HeLa cells was accompanied by a significant decrease in the level of the phosphorylated-Thr161 CDC2/p34 protein.

With the aim to provide further evidence for the inhibition of Hsp90α activity by compound **6**, its effects in HeLa cells on the client protein levels of Hsp90 were investigated by additional Western blot analysis. Compound **6** (10 and 20 μM) induced a significant depletion of pAkt and p-ERK1 proteins (Figure 3B), while the Hsp70 level was slightly affected after the treatment (Figure 3A). To investigate the possible effects of compound **6** on Hsp90α bioactivity, its ATPase enzymatic activity was also investigated. Radicicol and hypoestenonol B (**16**), showing no affinity towards the chaperone in the SPR studies, were selected as a positive and a negative control, respectively. ATPase activity of Hsp90α was affected by **6** at 5 and 10 μM (Figure 4), showing an inhibition almost comparable to that of radicicol.

To rationalize the biological effects of fusicoccane diterpenoid **6**, molecular docking studies were performed between **6** and Hsp90α protein. The ATP-bound active state of Hsp82, a yeast Hsp90α homologue (PDB code: 2CG9),[30] was used as a model receptor and its sequence alignment with the

human protein, as reported by Lee et al.,[31] was utilized as reference during a comparative experimental–computational analysis. The Induced Fit docking protocol[31,18] was used to account accurately for both ligand and receptor flexibility due to the high plasticity of Hsp90 during its mechanism of action. Starting from the biological evaluation reported above, the region at the interface between the *C*-terminal chains of Hsp90α homologue (Figure 5) was considered as the area of pharmacologic interest. From the structural point of view, **6** interacts with the chaperone structure as a result of two hydrogen bonds between the CO group at C-5 and the OH group at C-18 with $Gly675_{chainA}$ and $Leu671_{chainB}$, respectively, and by hydrophobic interactions of the fusicoccane diterpene skeleton with the side chains of chains A and B (Figure 5). Therefore, the computational analysis of interaction pattern of the Hsp90α/**6** complex suggests a *C*-terminal inhibition mode.[18,32] According to the molecular docking results, compound **6** did not induce any considerable upregulation of Hsp90 and Hsp70 protein levels, while Hsp90 *N*-terminal inhibition produced an increase in both these protein levels.[18,32]

In conclusion, using a SPR based screening procedure it was found that fusicoccane diterpenoid **6** can interact efficiently with Hsp90α; the binding properties and the anti-proliferative activity of this compound have been determined by in vitro and cell-based assays. This molecule may help to expand the Hsp90 *C*-terminal inhibition chemical space and serve as chemical scaffold for the possible design of new *C*-terminus inhibitors of this chaperone.

EXPERIMENTAL SECTION

General Experimental Procedures. Optical rotations were measured on a Rudolph Research Analytical Autopol IV polarimeter equipped with a sodium lamp (589 nm) and a 1 dm microcell. NMR experiments were performed on a Bruker DRX-600 spectrometer (BrukerBioSpinGmBH, Rheinstetten, Germany) equipped with a Bruker 5 mm TCI CryoProbe at 300 K. All 2D NMR

spectra were acquired in methanol-d_4 or $CDCl_3$, and standard pulse sequences and phase cycling were used for TOCSY, COSY, ROESY, NOESY, HSQC, and HMBC spectra. HRESIMS were acquired in the positive-ion mode on a LTQ Orbitrap XL instrument (Thermo Fisher Scientific). TLC was performed on precoated Kieselgel 60 F_{254} plates (Merck), and compounds were detected by spraying with $Ce(SO_4)_2/H_2SO_4$ solution. Column chromatography was performed over silica gel (70–220 mesh, Merck). Reversed-phase (RP) HPLC separations were conducted on a Waters 590 series pumping system equipped with a Waters R401 refractive index detector, using a C_{18} μ-Bondapak column (30 cm x 7.8 mm, 10 μm, Waters–Milford) and a mobile phase consisting of MeOH-H_2O mixtures at a flow rate of 2.0 mL/min.

Plant Material. The roots of *H. forsskaolii* were collected in Wadi Thee Ghazal near Taif in Saudi Arabia, in October 2012 (GPS coordinates 21°04'23.0"N 40°23'14.0"E). The plant was identified by Prof. Ammar Bader and the identification keys matched fully with Collenette.[1] A voucher specimen (number SA/IT-2012/2) was deposited at the herbarium of the Laboratory of Pharmacognosy, Faculty of Pharmacy at Umm Al-Qura University, Saudi Arabia.

Extraction and Isolation. The dried roots of *H. forsskaolii* (300 g) were powdered and extracted exhaustively using *n*-hexane (8.10 g), chloroform (5.5 g), chloroform-methanol (3.0 g), and methanol (15.3 g), by ASE 2000. Part of the chloroform extract (4.5 g) was subjected to column chromatography using silica gel and eluting with $CHCl_3$ followed by increasing concentrations of MeOH in $CHCl_3$ (between 1% and 100%). Fractions of 50 mL were collected, analyzed by TLC (silica gel plates, in $CHCl_3$ or mixtures $CHCl_3$-MeOH 99:1, 98:2, 97:3, 9:1, 4:1; $CHCl_3$-MeOH-H_2O 40:9:1), and grouped into nine pooled fractions (A-I). Fraction B (198 mg) was subjected to RP-HPLC with MeOH-H_2O (85:15) as eluent to give pure compounds **1** (1.9 mg, t_R = 21 min), **2** (1.5 mg, t_R = 24 min), and **3** (2.0 mg, t_R = 30 min). Fraction D (300 mg) was subjected to RP-HPLC with MeOH-H_2O (75:25) as mobile phase to yield compounds **2** (0.7 mg, t_R = 28 min), **9** (2.1 mg, t_R = 31 min) and **11** (3.4 mg, t_R = 52 min). Fractions E (274 mg) and F (336 mg) were subjected to semi-preparative reversed-phase HPLC (MeOH-H_2O, 65:35) to yield compounds **15** (2.9 mg, t_R = 10

min), **14** (3.5 mg, t_R = 20 min), and **4** (2.1 mg, t_R = 35 min), from fraction E, and compounds **5** (2.0 mg, t_R = 15 min) and **16** (4.5 mg, t_R = 33 min), from fraction F. Fraction G (250 mg) was subjected to RP-HPLC using MeOH-H_2O (1:1) to give the pure compounds **6** (1.8 mg, t_R = 30 min), **8** (1.4 mg, t_R = 27 min), and **10** (1.4 mg, t_R = 19 min). Part of the $CHCl_3$-MeOH (9:1) residue (2.0 g) was submitted to chromatographic separation on a Sephadex LH-20 column, using MeOH as mobile phase; fractions were collected, analyzed by TLC on silica 60 F_{254} gel-coated glass sheets with *n*-BuOH-CH_3COOH-H_2O (60:15:25) and $CHCl_3$-MeOH-H_2O (40:9:1), $CHCl_3$-MeOH (9:1), and grouped to obtain five major fractions (A-E). Fraction C (880 mg) was dissolved in $CHCl_3$ and separated on silica gel column, eluted with step gradients of $CHCl_3$-MeOH (100:0, 9:1, 8:2, 7:3, 1:1 and 0:100). Fractions of 25 mL were collected, analyzed by TLC and grouped into eight main fractions (C1-C8). Fraction C2 (30 mg) was subjected to RP-HPLC using MeOH-H_2O (7:3) to give pure compound **4** (1.4 mg, t_R = 12 min). Fraction C3 (74.5 mg) was purified RP-HPLC with MeOH-H_2O (3:2) to give the pure compounds **10** (1.5 mg, t_R = 14 min), **13** (3.8 mg, t_R = 31 min), and **12** (2.3 mg, t_R = 50 min). Fraction C4 (26.7 mg) was subjected to RP-HPLC using MeOH-H_2O (55:45) to give pure compound **10** (1.5 mg, t_R = 20 min). Fraction C5 (46.7 mg) was subjected to RP-HPLC using MeOH-H_2O (1:1) to give the pure compounds **7** (0.7 mg, t_R = 28 min), **8** (0.8 mg, t_R = 27 min), and **6** (3.9 mg, t_R = 30 min).

Compound (1): white amorphous powder; $[\alpha]_D^{25}$ +11.5 (*c* 0.1, MeOH); ^1H and ^{13}C NMR, see Table 1; HRESIMS *m/z* 309.2191 $[M + Na]^+$, (calcd for $C_{20}H_{30}ONa$ 309.2194).

Compound (2): white amorphous powder; $[\alpha]_D^{25}$ +21 (*c* 0.1, MeOH); ^1H and ^{13}C NMR, see Table 1; HRESIMS *m/z* 309.2178 $[M + Na]^+$, (calcd for $C_{20}H_{30}ONa$ 309.2194).

Compound (3): white amorphous powder; $[\alpha]_D^{25}$ +83 (*c* 0.1, MeOH); ^1H and ^{13}C NMR, see Table 1; HRESIMS *m/z* 289.2528 $[M + H]^+$, (calcd for $C_{20}H_{33}O$ 289.2531).

Compound (4): white amorphous powder; $[\alpha]_D^{25}$ +49 (*c* 0.1, MeOH); ^1H and ^{13}C NMR, see Table 1; HRESIMS *m/z* 315.1959 $[M + H]^+$, (calcd for $C_{20}H_{27}O_3$ 315.1960).

*Compound (**5**):* white amorphous powder; $[\alpha]_D^{25}$ +37 (*c* 0.1, MeOH); ^{1}H and ^{13}C NMR, see Table 2; HRESIMS *m/z* 341.2192 $[M + Na]^+$, (calcd for $C_{20}H_{30}O_3Na$ 341.2093).

*Compound (**6**):* white amorphous powder; $[\alpha]_D^{25}$ +92 (*c* 0.1, MeOH); ^{1}H and ^{13}C NMR, see Table 2; HRESIMS *m/z* 339.1931 $[M + Na]^+$, 317.2114 $[M + H]^+$, (calcd for $C_{20}H_{28}O_3Na$ 339.1936).

*Compound (**7**):* white amorphous powder; $[\alpha]_D^{25}$ +86 (*c* 0.1, MeOH); ^{1}H and ^{13}C NMR, see Table 2; HRESIMS *m/z* 339.1911 $[M + Na]^+$, (calcd for $C_{20}H_{28}O_3Na$ 339.1936).

*Compound (**8**):* white amorphous powder; $[\alpha]_D^{25}$ +53 (*c* 0.1, MeOH); ^{1}H and ^{13}C NMR, see Table 3; HRESIMS *m/z* 315.1960 $[M + H]^+$, (calcd for $C_{20}H_{27}O_3$ 315.1960).

*Compound (**9**):* white amorphous powder; $[\alpha]_D^{25}$ +92 (*c* 0.1, MeOH); ^{1}H and ^{13}C NMR, see Table 3; HRESIMS *m/z* 289.2528 $[M + H]^+$, (calcd for $C_{20}H_{33}O$ 289.2531).

*Compound (**10**):* white amorphous powder; $[\alpha]_D^{25}$ +29 (*c* 0.1, MeOH); ^{1}H and ^{13}C NMR, see Table 3; HRESIMS *m/z* 347.1855 $[M + H]^+$, (calcd for $C_{20}H_{27}O_5$ 347.1858).

Reagents and Antibodies. Fetal bovine serum (FBS) was from GIBCO (Life Technologies, Grand Island, NY, USA). Hsp90α was purchased from Tebu Bio Italy (Magenta, Milan, Italy) and bovine serum albumin (BSA) was from Sigma-Aldrich (Saint Louis, MO, USA). The antibody anti-Hsp90α (mouse monoclonal SPA-835) was obtained from Stress-gen Bio-reagents Corporation (Victoria, BC, Canada). The antibodies anti-Hsp70 (mouse monoclonal sc-32239), anti-cyclin A (rabbit polyclonal sc-596-G), anti-pAkt (rabbit polyclonal sc-7935-R), anti-Akt (rabbit polyclonal), anti-Mdm2 (rabbit polyclonal), anti-Cdc2 (mouse monoclonal, sc-8395) and anti-phospho (Thr161)-Cdc2 p34 (rabbit polyclonal, sc-101654), anti-Erk1/2 (mouse monoclonal sc-1647), anti-pErk (mouse monoclonal sc-7383), anti-α-tubilin (mouse monoclonal sc-32293), anti-GAPDH (rabbit polyclonal), were obtained from Santa Cruz Biotechnology (Santa Cruz Biotechnology, Inc., Delaware, CA, USA); anti-Raf1 (C-12) and anti-Egfr (rabbit polyclonal) were obtained from Cell Signaling Technologies, Danvers, MA, USA; appropriate peroxidase-conjugated secondary antibodies were from Jackson Immuno Research (Baltimore, PA, USA).

Surface Plasmon Resonance Analyses. SPR analyses were performed using a Biacore 3000 optical biosensor, equipped with research-grade CM5 sensor chips (GE Healthcare, Milano, Italy). Recombinant human Hsp90α (SPP-776, Stress-gen Bio-reagents Corporation, Victoria, Canada) was dissolved at 100 μg/mL in CH_3COONa 50 mM, pH 5.0) and immobilized on a CM5 sensor chip surface using standard amine-coupling protocols and flow rate of 5 μL/min, to obtain an optical density of 15 kRU. Compounds **1**-**6** and **8**-**16**, as well as 17-AAG and radicicol used as positive controls, were dissolved in 100% DMSO to obtain 4 mM solutions, and diluted 1:200 (v/v) in PBS (10 mM NaH_2PO_4, 150 mM NaCl, pH 7.4) to a final DMSO concentration of 0.1%. For each molecule, a five-point concentration series was set up, spanning 25 nM–50 nM–250 nM–1 μM–4 μM, and, for each sample, a complete binding study was carried out using triplicate aliquots. SPR experiments were performed at 25 °C, using a flow rate of 50 μL/min, with 60 s monitoring of association and 300 s monitoring of dissociation. Changes in mass, due to the binding response, were recorded as resonance units (RU). To obtain the dissociation constant (K_D), these responses were fit to a 1:1 Langmuir binding model by nonlinear regression, using the BiaEvaluation sofware program provided by GE Healthcare. Simple interactions were suitably fitted to a single-site bimolecular interaction model (A + B = AB), yielding a single K_D.

ATP Hydrolysis Inhibition. This assay was performed using the ATPase/GTPase Activity Assay Kit (MAK113-1KT) from Sigma-Aldrich, and following the manufacturer's instructions. ATPase hydrolysis was carried out for 3 h at 37 °C in Tris 40 mM pH 7.4, NaCl 80 mM, KCl 10 mM, $MgAc_2$ 8 mM, EDTA 1 mM, using Hsp90α 2.2 mg/mL (final concentration: 1 μM in 20 μL) and different concentrations of **6** (1 μM, 5 μM and 10 μM in 20 μL, final volume). Subsequently, ATP 4 mM was supplemented to each mixing solution for 40 min at room temperature, before adding 80 μL of malachite green reagent. ADP generation was measured after 30 min of incubation through a Thermofisher UV spectrophotometer (540 nm excitation and 620 nm emission). The absorbance intensity value measured in the absence of compound **6** was assumed as 100% of Hsp90α activity.

The background reaction rate was measured in a reaction lacking enzyme or substrate and subtracted from the experimental rates.

Cell Culture and Treatment. HeLa (cervical carcinoma) and Jurkat (T-cell lymphoma) cell lines were purchased from the American Type Cell Culture (ATCC) (Rockville, MD, USA). The cells were maintained in DMEM (HeLa) or RPMI 1640 (Jurkat), supplemented with 10% FBS, 100 mg/ L streptomycin and penicillin 100 IU/mL at 37 °C in a humidified atmosphere of 5% CO_2. To ensure logarithmic growth, cells were subcultured every two days. Stock solutions (50 mM) of purified compounds in DMSO were stored in the dark at 4 °C. Appropriate dilutions were prepared in culture medium immediately prior to use. In all experiments, the final concentration of DMSO did not exceed 0.15% (v/v).

Cell Viability and Cell Cycle. Cells were seeded in 96-well plates and incubated for 48 h in the absence (vehicle only) and in the presence of different concentrations of compounds (10 – 150 μM) and etoposide as positive control. The day before treatments, cells were seeded at a cell density of 1×10^4 cells/well. The number of viable cells was quantified by MTT ([3-(4,5-dimethylthiazol-2-yl)-2,5-diphenyl tetrazolium bromide]) assay. Absorption at 550 nm for each well was assessed using a microplate reader (LabSystems, Vienna, VA, USA). The cell viability was also checked by a Trypan Blue exclusion assay using a Bürker counting chamber. Half maximal inhibitory concentration (IC_{50}) values were calculated from cell viability dose–response curves and defined as the concentration resulting in 50% inhibition of cell survival as compared to controls. Human peripheral blood mononuclear cells (PBMC) were used to evaluate cytotoxic effects by trepan blue count of **6**. PBMC were isolated from buffy coats of healthy donors (kindly provided by the Blood Center of the Hospital of Battipaglia, Italy) by using standard Ficoll-Hypaque gradients. Freshly isolated PBMC contained 93.0 ÷ 2.9 % live cells, were incubated with DMSO or compound **6** at 50 and 100 μM for 48 h. The cell cycle was evaluated by propidium iodide (PI) staining of permeabilized cells, according to the available protocol, and flow cytometry (BD FACSCalibur flow cytometer, Becton Dickinson, San Jose, CA, USA).[33] Data from 5000 events per sample were

collected. The percentages of the elements in the hypodiploid region and in G_0/G_1, S and G_2/M phases of the cell cycle were calculated using the CellQuest and MODFIT software, respectively.

Statistical Analysis. Data reported are the mean values ± SD from at least three experiments, performed in duplicate, showing similar results. Differences between treatment groups were analyzed by Student's *t*-test. Differences were considered significant when $p < 0.05$.

Western Blot Analyses. Cell whole lysates (HeLa) for immunoblot analysis were prepared according to a standard protocol. Protein concentration was determined by a DC Protein Assay kit (Bio-Rad, Berkeley, CA, USA), using bovine serum albumin (BSA) as a standard. Proteins were fractionated on SDS-PAGE, transferred into nitrocellulose membranes, and immunoblotted with the appropriate primary antibody. Signals were visualized with the appropriate horseradish peroxidase-conjugated secondary antibody and enhanced chemiluminescence (Amersham Biosciences-GE Healthcare, NY, USA). Densitometry of bands was performed with ImageJ software (http://rsbweb.nih.gov/ij/download.html).

Computational Details. Maestro 10.2 (Maestro version 10.2, 2015) was used for generating the starting 3D chemical structure of one of the possible enantiomers of compound **6** (**6a** and **6b**, Chart 2). As a first step, exhaustive conformational searches of **6a** at the empirical MM level with the MCMM (50000 steps) and LMCS (50000 steps) methods were performed, in order to allow a full exploration of the conformational space. Furthermore, molecular dynamics simulations were performed at different temperatures (450, 600, 700, 750 K), with a time step of 2.0 fs, an equilibration time of 0.1 ns, and a simulation time of 10 ns. All the conformers were minimized using the OPLS force field[34] and the Polak-Ribier conjugate gradient algorithm. The "Redundant Conformer Elimination" module of Macromodel 10.2 was used to select non-redundant conformers that were used for the prediction of ECD spectra. The QM calculations were performed using Gaussian 09 software.[35] The conformers were optimized at the QM level using the MPW1PW91 functional and the 6-31G(d) basis set. The prediction of the ECD spectra were performed using all the significant conformers, and performing QM calculations at the TDDFT (NStates = 40)

MPW1PW91/6-31g(d,p) level in EtOH (IEFPCM) to reproduce the effect of the experimental solvent.[25] The final ECD spectra of **6a** was built considering the influence of each conformer on the total Boltzmann distribution and taking into account the relative energies, and was graphically plotted using SpecDis software.[36] In order to simulate the experimental ECD curve, a Gaussian band-shape function was applied with an exponential half-width (σ/γ) of 0.20 eV.

Molecular Docking Studies. Input Files Preparation for Docking. Protein 3D model of the ATP-bound active state of Hsp82, a yeast Hsp90α homologue (PDB code: 2CG9)[30] was prepared using the Schrödinger Protein Preparation Wizard workflow (Maestro version 10.2, 2015).[37] Briefly, water molecules that were found 5 Å or more away from heteroatom groups were removed and cap termini were included. Additionally, all hydrogen atoms were added, and bond orders were assigned. The resulting PDB files were converted to the MAE format. Chemical structure of **6** was built with Maestro's Build Panel (Maestro version 10.2, 2015)[37] and subsequently processed with LigPrep (LigPrep version 3.4, 2015) in order to generate all the possible tautomers and protonation states at a pH of 7.4 ± 1.0; the resulting ligands were finally minimized employing the OPLS 2005 force field.

Induced Fit Docking. Binding sites for the initial Glide docking phases (Glide Standard Precision Mode) of the Induced Fit Workflow[38-40] were calculated on the 2CG9 structure,[30] mapping onto a grid with dimensions of 36 Å (outer box) and 20 Å (inner box), centered on residues 628-630, 640–641, 670–675 (Hsp90 residues numbering as in the PDB entry 2CG9). Side chains of residues close to the docking outputs (within 8.0 Å of ligand poses) were reoriented using Prime (Prime version 3.7, Schrödinger 2015),[41] and ligands were redocked into their corresponding low energy protein structures (Glide Extra Precision Mode), considering inner boxes dimensions of 5.0 Å (outer boxes automatically detected), with the resulting complexes ranked according to GlideScore.

ASSOCIATED CONTENT

Supporting Information. HRESIMS and NMR spectra of compounds **1-10** and IC_{50} values of compounds **1-6** and **8-16** against Jurkat and HeLa cell lines. This material is available via the Internet at http://pubs.acs.org.

AUTHOR INFORMATION

Corresponding Author

* Tel: +39-089-969754. Fax: +39-089-969602. E-mail: detommasi@unisa.it

ORCID[ID]

Giuseppe Bifulco: 0000-0002-1788-5170

Alessandra Braca: 0000-0002-9838-0448

Nunziatina De Tommasi: 0000-0003-1707-4156

Author contributions

[#]Equally contributing authors.

Notes

The authors declare no competing financial interest.

ACKOWLEDGEMENTS

This work was financially supported by the National Plan for Science, Technology, and Innovation (MAARIFAH) King Abdulaziz City for Science and Technology, Kingdom of Saudi Arabia (award number 12-MED2310-10) through Science and Technology Unit (STU) at Umm Al-Qura University.

REFERENCES

(1) Collenette, S. *Wildflowers of Saudi Arabia*; National Commission for Wildlife Conservation and Development: Riyadh, 1999; p 7.

(2) Balkwill, K.; Norris, F. G. *S. Afr. J. Bot*. **1985**, *51*, 133–144.

(3) Ghushash, A. *Plants of the mountains of Sarat and Hejaz*; Sarawat Press: Jeddah, 2006; Vol. 2, pp 550–554.

(4) Muhammad, I.; Mossa, J. S.; Al-Yahya, M. A.; El-Feraly, F. S.; McPhail, A. T. *Phytochemistry* **1997**, *44*, 125–129.

(5) Muhammad, I.; Mossa, J. S.; Ramadan, A. F.; El-Feraly, F. S.; Hufford, C. D. *Phytochemistry* **1998**, *47*, 1331–1336.

(6) Al Musayeib, N. M.; Mothana, R. A.; Mohamed, G. A.; Ibrahim, S. R. M.; Maes, L. *Phytochem. Lett.* **2014**, *10*, 23–27.

(7) Minami, A.; Ozaki, T.; Liu, C.; Oikawa, H. *Nat. Prod. Rep*. **2018**, *35*, 1330–1346.

(8) Okogun, J. I.; Adesomoju, A. A.; Adesida, G. A., Lindner, H. J.; Habermehl, G. *Z. Naturforsch.* **1982**, *37c*, 558–561.

(9) Rasoamiaranjanahary, L.; Guilet, D.; Marston, A.; Randimbivololona, F.; Hostettmann, K. *Phytochemistry* **2003**, *64*, 543–548.

(10) Wu, X. D.; Luo, D.; Tu, W. C.; Deng, Z. T.; Chen, X. J.; Su, J.; Ji, X.; Zhao, Q. S. *Org. Lett*. **2016**, *18*, 6484–6487.

(11) Gilabert, M.; Ramos, A. N.; Schiavone, M. M.; Arena, M. E.; Bardon, A. *J. Nat. Prod*. **2011**, *74*, 574–579.

(12) Zheng, D.; Han, L.; Qu, X.; Chen, X.; Zhong, J.; Bi, X.; Liu, J.; Jiang, Y.; Jiang, C.; Huang, X. *J. Nat. Prod.* **2017**, *80*, 837–844.

(13) Tatokoro, M.; Koga, F.; Yoshida, S.; Kihara K. *EXCLI J*. **2015**, *14*, 48–58.

(14) Jhaveri, K.; Taldone, T.; Modi, S.; Chiosis, G. *Biochim. Biophys. Acta* **2012**, *1823*, 742–755.

(15) Solárová, Z.; Mojžiš, J.; Solár P. *Int. J. Oncol.* **2015**, *46*, 907–926.

(16) Alam, Q.; Alam, M. Z.; Sait, K. H. W.; Anfinan, N.; Noorwali, A. W.; Kamal, M. A.; Khan, M. S. A.; Haque, A. *Curr. Drug. Metab*. **2017**, *18*, 868–876.

(17) Wang, Y.; Jin, F.; Wang, R.; Li, F.; Wu, Y.; Kitazato, K.; Wang, Y. *Arch. Virol.* **2017**, *162*, 3269–3282.

(18) Chini, M. G.; Malafronte, N.; Vaccaro, M. C.; Gualtieri, M. J.; Vassallo, A.; Vasaturo, M.; Castellano, S.; Milite, C.; Leone A.; Bifulco, G.; De Tommasi, N.; Dal Piaz F. *Chem.-Eur. J.* **2016**, *22,* 13236–13250.

(19) Dal Piaz, F.; Vassallo, A.; Chini, M. G.; Cordero, F. M.; Cardona, F.; Pisano, C.; Bifulco, G.; De Tommasi, N.; Brandi, A. *PLoS One* **2012**, *7*, e43316.

(20) Dal Piaz, F.; Malafronte, N.; Romano, A.; Gallotta, D.; Belisario, M. A.; Bifulco, G.; Gualtieri, M. J.; Sanogo, R.; De Tommasi, N.; Pisano, C. *Phytochemistry* **2012**, *75*, 78–89.

(21) El Sayed, K. A. *J. Nat. Prod*. **2001**, *64*, 373–375.

(22) Nadmid, S.; Plaza, A.; Lauro, G.; Garcia, R.; Bifulco, G.; Muller, R. *Org. Lett.* **2014**, *16*, 4130–4133.

(23) Khalfaoui, A.; Chini, M. G.; Bouheroum, M.; Belaabed, S.; Lauro, G.; Terracciano, S.; Vaccaro, M. C.; Bruno, I.; Benayache, S.; Mancini, I.Bifulco, G. *J. Nat. Prod.* **2018**, *81*, 1786–1794.

(24) Di Micco, S.; Chini, M. G.; Riccio, R.; Bifulco, G. In *Handbook of Marine Natural Products*; *Quantum Chemical Calculation of Chemical Shifts in the Stereochemical Determination of Organic Compounds: A Practical Approach;* Fattorusso, E., Gerwick, W. H., Taglialatela-Scafati, O., Eds.; Spinger: Berlin, 2012; pp 571–599.

(25) Tomasi, J.; Mennucci, B.Cammi, R. *Chem. Rev.* **2005**, *105*, 2999–3093.

(26) Muñoz Camero, C.; Vassallo, A.; De Leo, M.; Temraz, A.; De Tommasi, N.; Braca A. *Planta Med*. **2018**, *84*, 964–970.

(27) Mosmann, T. *J. Immunol. Methods* **1983**, *65*, 55–63.

(28) Karkoulis, P. K.; Stravopodis, D. J.; Konstantakou, E. G.; Voutsinas, G. E. *Cancer Cell Int.* **2013**, *13*, 11.

(29) Suzuki, R.; Hideshima, T.; Mimura, N.; Minami, J.; Ohguchi, H.; Kikuchi, S.; Yoshida, Y.; Gorgun, G.; Cirstea, D.; Cottini, F.; Jakubikova, J.; Tai, Y. T.; Chauhan, D.; Richardson, P. G.; Munshi, N. C.; Utsugi, T.; Anderson K. C. *Leukemia* **2015**, *29*, 510–514.

(30) Ali, M. M. U.; Roe, S. M.; Vaughan, C. K.; Meyer, P.; Panaretou, B.; Piper, P. W.; Prodromou, C.; Pearl, L. H. *Nature* **2006**, *440*, 1013–1017.

(31) Lee, C. C.; Lin, T. W.; Ko, T. P.; Wang, A. H. *PloS One* **2011**, *6*, e19961.

(32) Terracciano, S.; Russo, A.; Chini, M. G.; Vaccaro, M. C.; Potenza, M.; Vassallo, A.; Riccio, R.; Bifulco, G.; Bruno, I. *Sci. Rep.* **2018**, *8*, 1709.

(33) Hernandez V.; De Leo, M.; Cotugno, R.; Braca, A.; De Tommasi, N.; Severino L. *Planta Med*. **2018**, *84*, 716–720.

(34) Piazza, G.; Fanikos, J.; Zayaruzny, M.; Goldhaber, S. Z. *Thromb. Haemost.* **2009**, *102*, 505–510.

(35) Frisch, M. J. T., G. W.; Schlegel, H. B.; Scuseria, G. E.; Robb, M. A.; Cheeseman, J. R.; Scalmani, G.; Barone, V.; Mennucci, B.; Petersson, G. A.; Nakatsuji, H.; Caricato, M.; Li, X.; Hratchian, H. P.; Izmaylov, A. F.; Bloino, J.; Zheng, G.; Sonnenberg, J. L.; Hada, M.; Ehara, M.; Toyota, K.; Fukuda, R.; Hasegawa, J.; Ishida, M.; Nakajima, T.; Honda, Y.; Kitao, O.; Nakai, H.; Vreven, T.; Montgomery, J. A., Jr.; Peralta, J. E.; Ogliaro, F.; Bearpark, M.; Heyd, J. J.; Brothers, E.; Kudin, K. N.; Staroverov, V. N.; Kobayashi, R.; Normand, J.; Raghavachari, K.; Rendell, A.; Burant, J. C.; Iyengar, S. S.; Tomasi, J.; Cossi, M.; Rega, N.; Millam, J. M.; Klene, M.; Knox, J. E.; Cross, J. B.; Bakken, V.; Adamo, C.; Jaramillo, J.; Gomperts, R.; Stratmann, R. E.; Yazyev, O.; Austin, A. J.; Cammi, R.; Pomelli, C.; Ochterski, J. W.; Martin, R. L.; Morokuma, K.; Zakrzewski, V. G.; Voth, G. A.; Salvador, P.; Dannenberg, J. J.; Dapprich, S.; Daniels, A. D.; Farkas, Ö.; Foresman, J. B.; Ortiz, J. V.; Cioslowski, J.; Fox, D. J. *Gaussian 09, Revision A.02*, Gaussian, Inc., Wallingford CT, 2009.

(36) Bruhn, T.; Schaumloffel, A.; Hemberger; Y.; Bringmann, G. *Chirality* **2013**, *25*, 243–249.

(37) Maestro version 10.2, Schrödinger, LLC, New York, NY, 2015.

(38) Induced Fit Docking, Protocol 2015-2, Glide version 6.4, Prime version 3.7, Schrödinger, LLC, New York, NY, 2015.

(39) Sherman, W.; Beard, H. S.; Farid, R. *Chem. Biol. Drug Des.* **2006**, *67*, 83–84.

(40) Sherman, W.; Day, T.; Jacobson, M. P.; Friesner, R. A; Farid, R. *J. Med. Chem.* **2006**, *49*, 534–553.

(41) LigPrep version 3.4, Schrödinger, LLC, New York, NY, 2015.

Chart 1

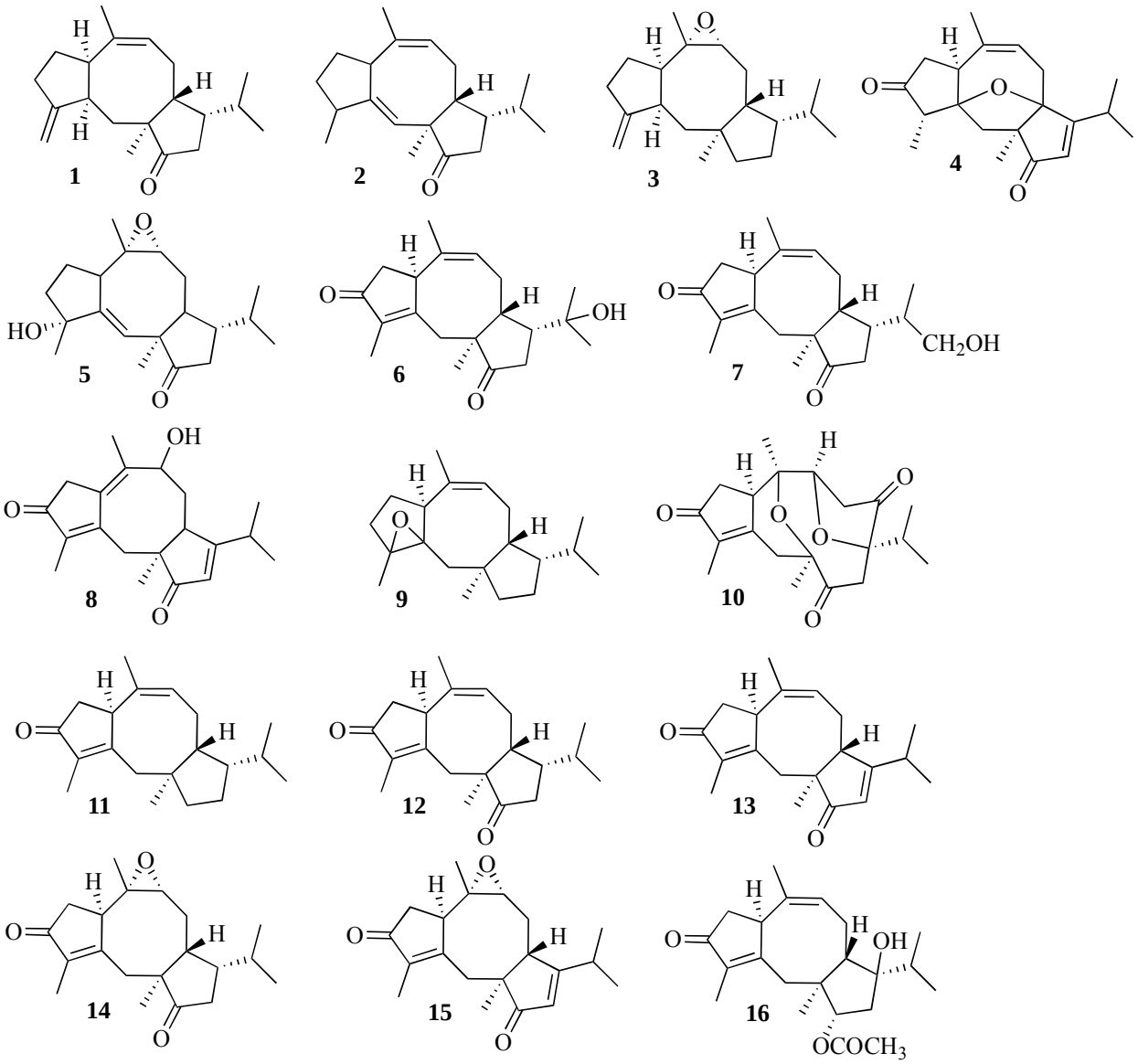

Chart 2

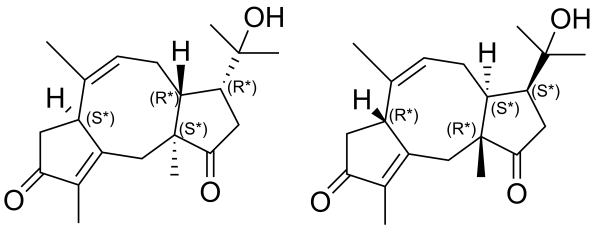

6a **6b**

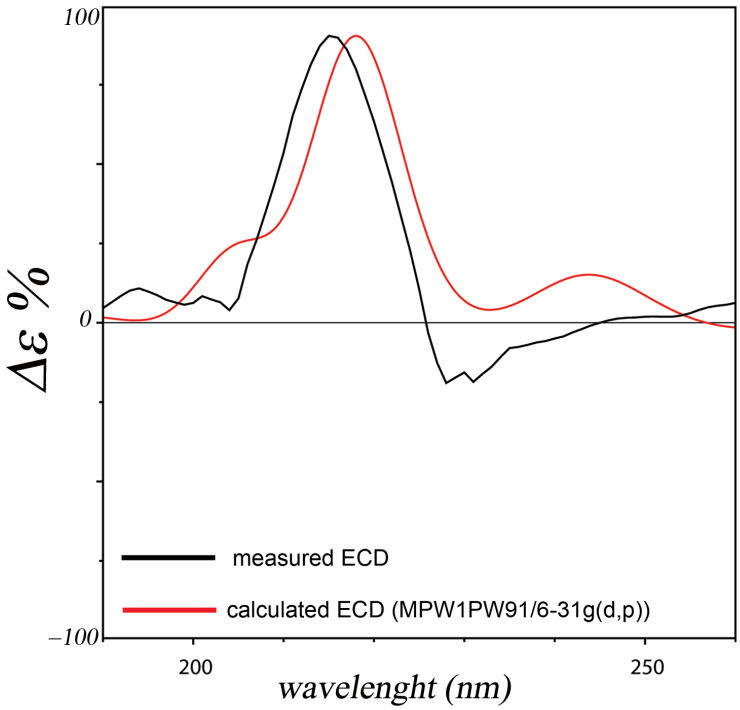

Figure 1. Comparison of the experimental ECD spectra of **6** with the TDDFT-predicted curves of compounds **6a**.

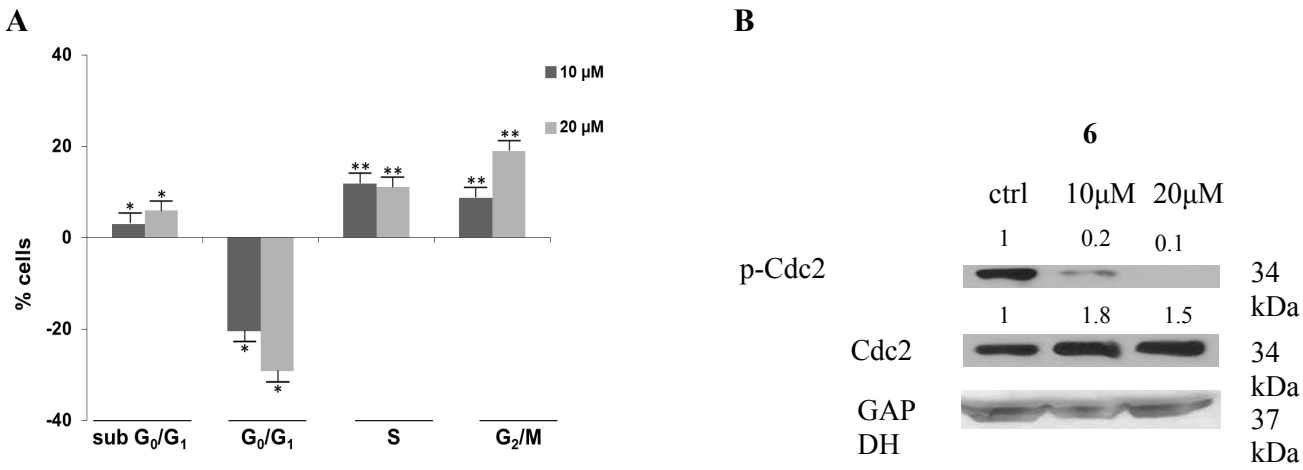

Figure 2. Effect of **6** on cell cycle progression and on cell cycle regulatory protein levels. (A) Flow cytometric evaluation of DNA content in HeLa cells treated with DMSO (control) or **6** (10 and 20 μM) for 48 h. On the y-axis: the percentages of cells in subG_0G_1 (hypodiploidia) and in each cell cycle phase of **6**-treated cells subtracted for the corresponding percentages of control cells. Results are expressed as means ± SD of three experiment performed in duplicate (**$p < 0.005$, *$p < 0.5$). (B) Western Blot analysis of Cdc2 and pCdc2 (Thr161) levels in HeLa cells treated with DMSO (ctrl) or **6** (10 and 20 μM) for 48 h. For each immunoblot, band intensity was quantified by densitometry (numbers above each lane). GAPDH was included as a loading control. The blots are representative of at least two different experiments with similar results.

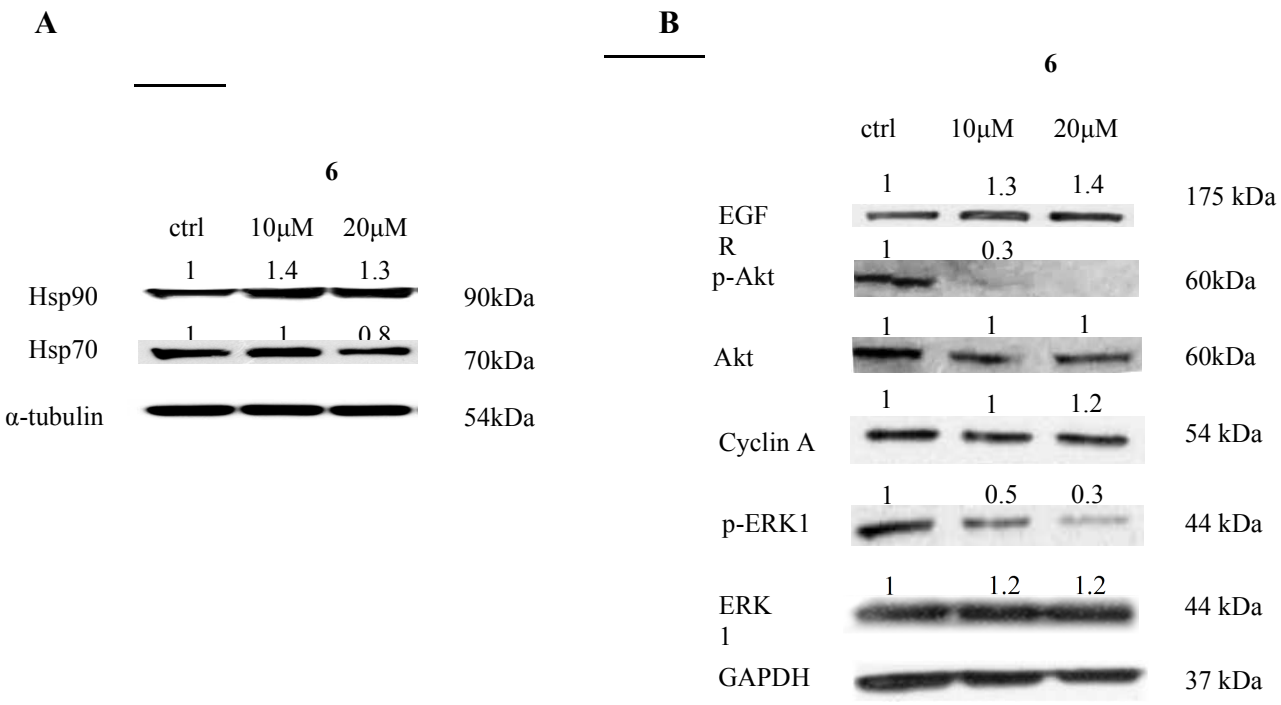

Figure 3. Effect of **6** on Hsp90α client proteins levels in HeLa cells after treatment with **6** (10 and 20 μM) for 48 h. Equal amounts (30 μg) of total protein lysate were separated on SDS-PAGE and client proteins were visualized by Western blot analysis. α-tubulin and GAPDH were used as loading controls. The blots are representative of three different experiments with similar results. Numbers above each lane represent the densitometric values.

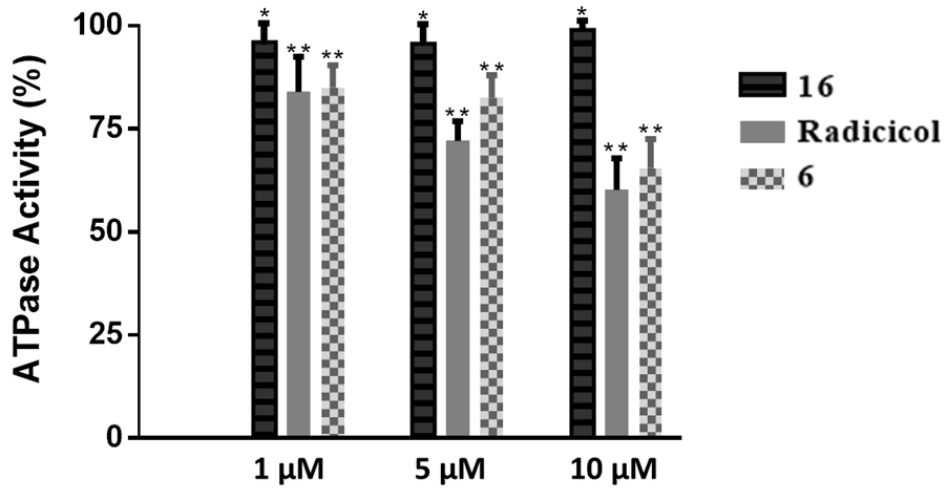

Figure 4. Effect of compound **6** on Hsp90α ATPase activity. Inhibition of the ATPase activity of Hsp90α treated with DMSO (control) or different concentrations of **6**, radicicol (positive control), and **16** (negative control). Data are the means ± SD of two independent experiments performed in triplicate. *$p < 0.05$, **$p < 0.005$.

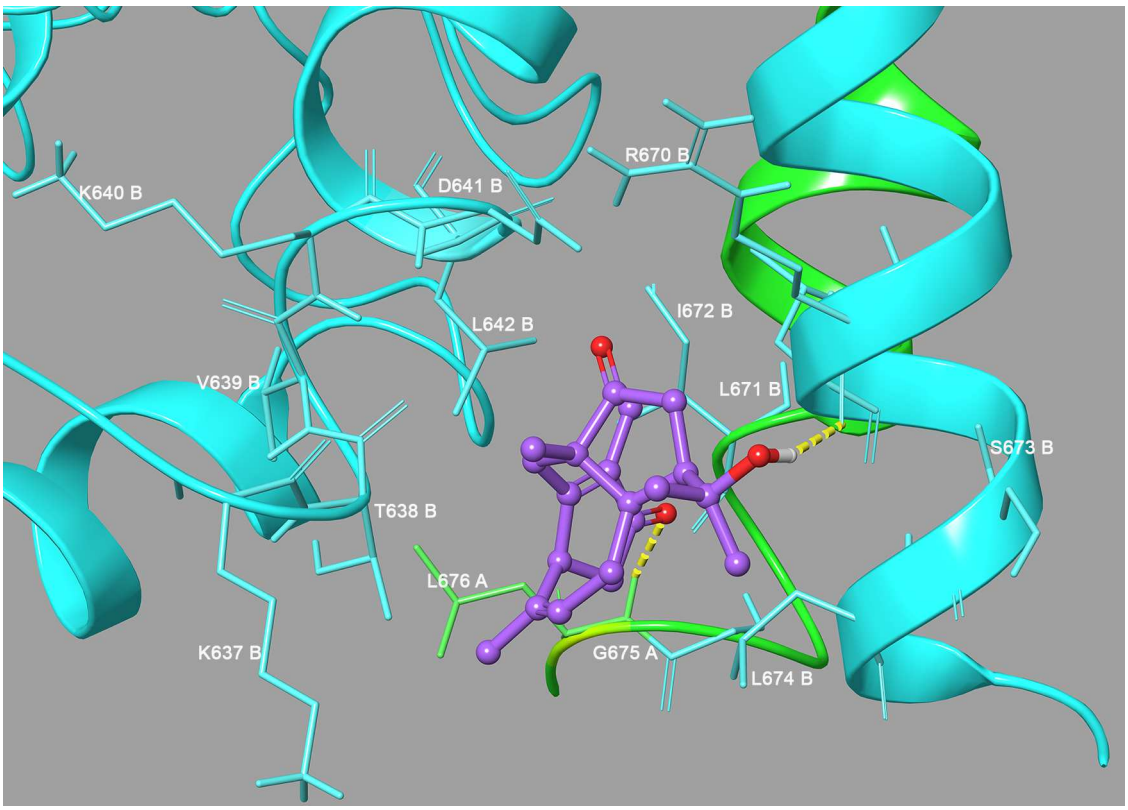

Figure 5. Three-dimensional models of **6** (violet sticks) with the *C*-terminal domain of the Hsp82 yeast analogue of Hsp90α (chain A is depicted in green and chain B in cyan).

Table 1. ^{1}H and ^{13}C NMR Data of Compounds **1-4** (CD_3OD, 600 MHz)[a]

position	**1**		**2**		**3**		**4**[b]	
	δ_H	δ_C	δ_H	δ_C	δ_H	δ_C	δ_H	δ_C
1		51.4		54.0		50.0		58.6
2a	2.29 dd (15.0, 5.0)	35.0	5.59 s	127.5	2.15 dd (14.0, 4.0)	42.0	2.40 d (15.0)	42.3
2b	0.89 dd (15.0, 12.0)				1.18 dd (14.0, 12.0)		1.77 d (15.0)	
3	2.56[c]	47.7		157.5	2.56[c]	48.7		92.1
4		148.0	2.53 m	40.3		157.0	2.22[c]	53.2
5a	2.57[c]	31.9	1.93[c]	35.0	2.52[c]	30.8		215.8
5b	2.45 br t (10.0)		1.47 m		2.46 br t (10.5)			
6a	1.96[c]	26.0	1.93[c]	29.6	1.92[c]	26.0	2.67[c]	42.3
6b	1.95[c]		1.70 m		1.89[c]		2.20[c]	
7	3.31[c]	42.9	3.82 br d (8.3)	43.2	2.30 m	48.0	2.54 dd (10.5, 8.0)	53.8
8		137.1		142.7		62.8		136.0
9	5.51 t (8.3)	127.9	5.40 t (7.6)	127.7	2.80 dd (10.0, 5.3)	68.1	5.53 br d (7.0)	121.0
10a	2.54[c]	26.3	2.87 ddd (16.0, 8.6, 8.0)	25.9	2.22 br dd (14.0, 5.3)	26.0	2.88 br d (17.0)	33.1
10b	2.23 dd (13.2, 7.6)		2.34[c]		1.37 br dd (14.0, 10.0)		2.26 dd (17.0, 7.5)	
11	1.92[c]	56.6	2.18 br t (8.3)	52.7	1.77 br t (11.0)	50.8		95.2
12	1.94[c]	45.0	2.05 m	45.7	2.12 m	44.0		183.9
13a	2.42[c]	43.0	2.40 br d (18.0)	42.9	1.66 br ddd (11.0, 8.0, 3.0)	24.4	5.79 s	125.2
13b			2.34[c]		1.54[c]			
14a		225.0		225.0	1.56[c]	44.6		213.0
14b					1.48 m			
15	1.05 s	16.0	1.26 s	20.1	0.89 s	17.0	1.28 s	21.0
16a	4.79 s	103.1	1.03 d (7.0)	24.6	4.83 s	103.2	0.86 d (6.8)	6.2
16b	4.71 s				4.77 s			
17	1.57 s	21.9	1.76 s	20.3	1.09 s	20.0	1.85 s	27.7
18	1.86 m	32.3	1.80 m	30.5	1.89 m	29.0	2.65[c]	28.5
19	0.95 d (6.5)	23.7	0.94 d (6.7)	25.6	0.82 d (6.5)	18.9	1.19 d (6.5)	22.0
20	1.08 d (6.5)	24.0	1.08 d (6.7)	22.0	0.89 d (6.5)	23.3	1.15 d (6.5)	20.7

[a]*J* values are in parentheses and reported in Hz; chemical shifts are given in ppm; assignments were confirmed by COSY, 1D-TOCSY, HSQC, and HMBC experiments. [b]Data measured in $CDCl_3$. [c]Overlapped signal.

Table 2. ^{1}H and ^{13}C NMR Data of Compounds **5-7** (CD_3OD, 600 MHz)[a]

position	**5**		**6**		**7**	
	δ_H	δ_C	δ_H	δ_C	δ_H	δ_C
1		53.0		51.0		50.0
2a	6.32 s	133.0	3.34[b]	37.9	3.30[b]	37.7
2b			1.91 d (14.0)		1.94 d (16.0)	
3		149.8		176.6		174.7
4		80.0		139.0		140.0
5a	1.92[b]	41.5		211.0		211.0
5b	1.82[b]					
6a	2.09 m	25.9	2.51 br d (3.8)	37.6	2.52 br d (3.7)	37.7
6b	1.95[b]					
7	2.70 br d (8.6)	45.8	4.15 br s	43.9	4.15 br s	43.9
8		65.3		127.0		135.5
9	2.93 dd (9.0, 6.0)	66.0	5.76 t (7.0)	130.6	5.76 t (7.0)	129.6
10a	2.55 dd (15.0, 7.0)	26.9	2.83 br dd (13.0, 7.3)	26.3	2.83 br dd (14.6, 3.0)	26.5
10b	1.90[b]		2.72 m		2.43 br dd (14.6, 7.8)	
11	2.40 m	47.0	2.33 br dd (10.0, 8.0)	54.3	2.22 ddd (11.0, 7.8, 3.0)	55.8
12	2.16 m	44.0	2.47 m	47.9	2.15 m	41.9
13a	2.46 dd (16.5, 3.0)	42.5	2.67 dd (10.5, 10.0)	40.6	2.64 br d (18.0)	42.8
13b	2.43 dd (16.5, 8.0)		2.42 t (10.0)		2.50 dd (18.0, 7.0)	
14		223.0		220.0		222.4
15	1.11 s	18.0	1.17 s	17.0	1.01 s	16.3
16	1.40 s	27.7	1.75 s	9.6	1.72 s	8.6
17	1.19 s	20.0	1.52 s	18.0	1.56 s	17.8
18	1.81[b]	30.5		73.4	1.80 m	39.4
19a	1.10 d (6.6)	24.0	1.36 s	30.4	3.56 dd (11.0, 3.0)	67.7
19b					3.38 dd (11.0, 6.0)	
20	0.94 d (6.6)	22.0	1.28 s	30.4	1.17 s	19.2

[a]*J* values are in parentheses and reported in Hz; chemical shifts are given in ppm; assignments were confirmed by COSY, 1D-TOCSY, HSQC, and HMBC experiments. [b]Overlapped signal.

Table 3. ^{1}H and ^{13}C NMR Data of Compounds **8-10** (CD_3OD, 600 MHz)[a]

position	**8**		**8**[b]		**9**		**10**	
	δ_H	δ_C	δ_H	δ_C	δ_H	δ_C	δ_H	δ_C
1		55.0		55.0		36.0		81.0
2a	3.10 d (14.0)	40.0	3.00[c]	41.5	1.71[c]	42.1	3.54 d (14.5)	35.2
2b	2.90 d (14.0)	149.8	3.00[c]	149.8	1.52[c]		2.54 d (14.5)	
3		164.1		164.2		63.4		171.9
4		144.0		144.0		69.0		138.1
5a		204.0		204.9	1.98 br dd (14.0, 7.7)	33.0		210.0
5b					1.68[c]			
6a	3.53 d (12.8)	31.6	3.49 d (13.0)	32.0	1.50[c]	21.4	2.40 dd (18.0, 10.0)	37.2
6b	3.49 d (12.8)		3.28 d (13.0)		1.38[c]		2.14 br d (18.0)	
7		131.2		131.3	3.18 dd (10.0, 8.0)	43.8	3.57 br s	39.7
8		138.0		138.2		131.0		84.4
9	4.81 br s	74.5	4.78 br s	75.0	5.68 br d (7.0)	124.4	4.18 br s	79.7
10a	2.13[c]	27.8	2.14 m	27.8	2.21[c]	24.7	2.83 dd (14.0, 3.0)	38.2
10b	2.12[c]		2.07 m		2.14 dd (14.0, 7.5)		2.61 dd (14.0, 7.0)	
11	3.03 m	47.0	3.03 m	47.1	1.69[c]	56.6		215.0
12		188.0		186.1	2.23[c]	49.0		85.5
13a	5.84 s	121.5	5.78 s	122.3	1.59[c]	23.7	3.40 d (15.0)	44.7
13b					1.51[c]		2.73 d (15.0)	
14a		213.0		213.0	1.59[c]	44.3		211.3
14b					1.48[c]			
15	1.18 s	20.1	1.16[c]	21.0	0.95 s	18.7	1.29 s	27.1
16	1.80 s	7.9	1.91 s	9.2	1.36 s	16.0	1.72 s	8.4
17	1.96 s	23.4	1.96 s	24.6	1.66 s	20.0	0.86 s	19.4
18	2.62 m	29.0	2.53 m	29.3	1.90 m	29.6	1.75 m	39.3
19	1.00 br s	22.0	1.09 d (6.5)	21.7	0.92 d (6.5)	23.8	1.00 d (6.5)	16.7
20	1.18 d (6.5)	21.8	1.16[c]	21.0	0.84 d (6.5)	20.5	1.00 d (6.5)	17.0

[a]*J* values are in parentheses and reported in Hz; chemical shifts are given in ppm; assignments were confirmed by COSY, 1D-TOCSY, HSQC, and HMBC experiments. [b]Data measured in $CDCl_3$. [c]Overlapped signal.

Table 4. Thermodynamic Constants Measured by Surface Plasmon Resonance for the Interaction between the tested Compounds and Immobilized Hsp90α

compound	K_D (nM)[a]
1	401 ± 4
2	20.5 ± 1.2
3	130 ± 1
4	217 ± 17
5	45 ± 4
6	15.3 ± 0.2
8	no binding
9	no binding
10	120 ± 1
11	28 ± 3
12	1000 ± 25
13	1739 ± 75
14	no binding
15	no binding
16	no binding
radicicol	1.2 ± 0.1
17-AAG	388 ± 89

[a]Results are given as means ± standard deviation.

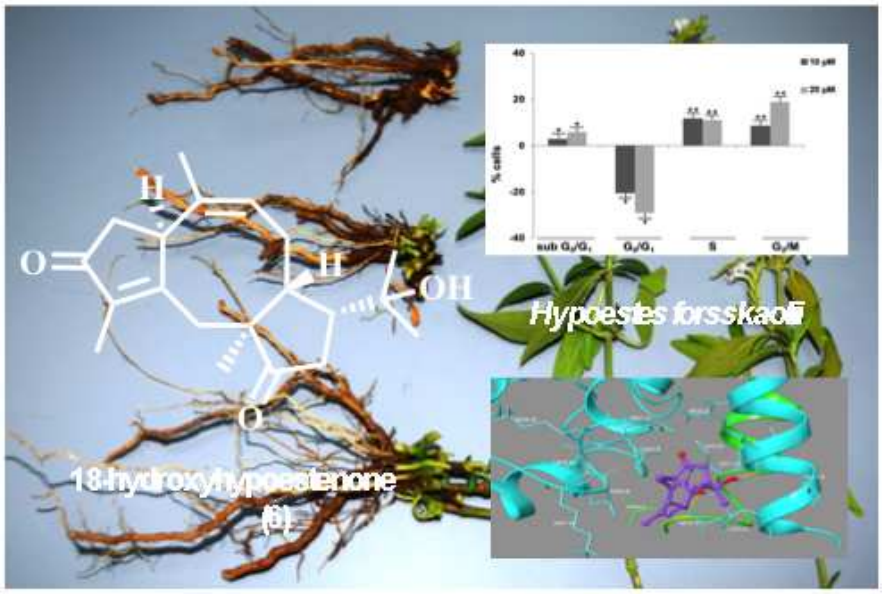
H
O
H
OH
O
18-hydroxyhypoestenone
(6)
Hypoestes forsskaolii